Exploring Semi-active TMD performance on lively footbridges considering Human-Structure Interaction in vertical direction

J.M. Soria

Department of Continuum Mechanics and Theory of Structures, ETSICCP, Universidad Politécnica de Madrid 28040 – Madrid, Spain
jm.soria@upm.es

J. F. Jiménez-Alonso

Department of Continuum Mechanics and Theory of Structures, Universidad de Sevilla, 41012 – Seville, Spain
jfjimenez@us.es

C. M. C. Renedo

Department of Continuum Mechanics and Theory of Structures, ETSICCP, Universidad Politécnica de Madrid 28040 – Madrid, Spain
carlos.martindelaconcha@upm.es

C. Gallegos-Calderón

Department of Continuum Mechanics and Theory of Structures, ETSICCP, Universidad Politécnica de Madrid 28040 – Madrid, Spain
christian.gallegos@upm.es

Human-Structure Interaction (HSI) can significantly influence the dynamic characteristics of pedestrian footbridges, particularly those distinguished by their lightness and slenderness. This study examines the performance of Tuned Mass Dampers (TMD) and Semi-Active Tuned Mass Dampers (STMD) on pedestrian footbridges when their modal parameters change due to the influence of HSI. For this purpose, a 30 m long simply-supported footbridge with linear mass values ranging from 200 to 2000 kg/m and a fundamental frequency varying from 1 to 5 Hz has been considered. In addition, several pedestrian streams with different pedestrian densities have been used to assess the structural dynamic response. The analysis highlights that structural lightness and slenderness are critical factors in determining whether the incorporation of an HSI model is relevant to accurately predict the dynamic performance of the structure. The findings indicate that while TMDs can become ineffective due to shifts in natural frequencies caused by HSI, resulting in a degradation of vibration reduction from 70-75% to 40-45%, STMDs demonstrate a robust capability to adjust and cope with these frequency changes, maintaining a higher average vibration reduction of around 55-60%. Consequently, STMDs emerge as a necessary solution for very slender structures where HSI significantly alters the global frequency response. This study highlights the importance of considering HSI in the design and implementation of damping solutions to ensure optimal functionality and user comfort on lightweight pedestrian bridges.

Keywords: footbridges; human-structure interaction; vibration control; dynamic behaviour; TMD techniques.

1. Introduction

Human-induced vibrations (HIV) in lightweight low-damped footbridges have been extensively studied for more than 20 years due to the discomfort experienced by users on the Millenium Bridge on its opening day.[1] Since then, the vibration serviceability limit state (VSLS) of footbridges subjected to pedestrian activities has become an additional requirement that must be met in order to ensure adequate structural performance. Several experimental campaigns and numerical analyses have been carried out to assess the effects of pedestrian activities on the dynamic response of footbridges.[2] From data collected from laboratory structures and in-service footbridges, the first generation of load models was established to predict acceleration levels in lightweight structures in several design guidelines.[3,4] By applying these models, in which pedestrian activities are defined as external loads acting on the structure, a good agreement between the test results and the numerical predictions was obtained for bridges built with traditional materials, such as steel or concrete.[5]

The methodology adopted even in recent design codes[6,7] presents the drawback of considering pedestrians as non-interacting external dynamic acting on the structure. Nowadays, the innovation on construction processes[8] and the inclusion of non-traditional materials, such as fiber reinforced polymers[9] or aluminum alloys,[10] in Bridge Engineering have shown that external load models overstimate the predicted structural reponse of footbridge at VSLS. Several studies have pointed out that modelling humans that interact with the structure is a step forward in the search for a more realistic design approach. The most common way of reproducing an interactive pedestrian in vertical direction is to model it as a mass-spring-damper-load system that moves through the structure.[11–14] Therefore, Human-Structure Interaction (HSI) can be considered an improvement to predict more accurately the dynamic response of a footbridge when checking its VSLS.[15–18] By adopting this modelling approach, it is evident that the dynamic parameters of a bare footbridge change when loaded with a pedestrian stream. Indeed, the presence of pedestrians affects at least the effective modal mass and associated damping ratio of a vibrating system.[19] This leads to a more precise assessment of the overall vibration levels in comparison with the model of pedestrians considered only as external loads. Recent studies by Colmenares et al. have further validated the analytical expressions for the frequency response function of coupled pedestrian-bridge systems considering HSI.[20,21]

The HSI effect is not only an important factor to consider when computing the response of lightweight footbridges, but also, when designing inertial vibration controllers for them.[22] Tuned Mass dampers (TMDs) are the most commonly passive inertial devices used in footbridges to cope with HIV.[5,23] They consist of a mass-spring-damper system attached to the structure to be controlled and tuned to one of its critical vibration modes.[24,25] When installed in lightweight footbridges, these controllers may suffer from detuning when the modal parameters of the structure

change, for example when the structure is loaded with interactive pedestrians. In addition, the modal parameters of the footbridge do not have a fixed value during the footbridge overall life cycle due to environmental and operational changes, and these variations may also produce detunning issues in the controllers.[26]

Generally, if the structure is not overly lightweight, the impact of HSI on its modal parameters is likely to be minimal, suggesting that a TMD could be a suitable solution,[27] even though it may still affect the structure's overall response. A good example of such a footbridge is the one studied by Fouli and Cámara,[27] in which the fundamental mode of vibration engages 81% of the total mass of the bridge which $133 \cdot 10^3$ kg. However, as the structure becomes lighter, the HSI effect becomes more significant, leading to greater uncertainty as a result of shifts in the structure's modal parameters.

Recently, adaptive control and adaptive TMDs have gained prominence as solutions that are less susceptible to detuning caused by HSI.[28,29] These adaptive TMDs are able to adjust one of their mechanical parameters, such as mass or stiffness, to achieve a re-tuned state when a significant change of the structure's natural frequency is detected. A good example of this type is the adaptative variable-mass TMD proposed by Wang[29], which adjusts its mass based on the structural frequency identified using wavelet transform. Another example is the adaptive variable-stiffness TMD discussed in recent studies,[30] which adjusts its stiffness and damping properties to retune to the structural natural frequency. However, adaptive devices adjust their properties gradually, which means that their response to fluctuations in the pedestrian stream over the structure is not immediate, reducing effectiveness when facing abrupt changes in modal parameters.[31] In these scenarios, the use of semi-active devices that are able to change their mechanical properties in real-time may become a competitive alternative.[32–34]

Under changing circumstances, Semi-active TMDs (STMDs) may offer a better performance than TMDs in terms of vibration control[35–37] and at a competitive cost. The dynamic performance of this non-linear system has been studied by several researches, and different devices oriented to mitigate excessive vibrations arise from pedestrian actions have been proposed over the years.[38] While previous studies have addressed the effect of HSI using adaptive TMDs in footbridges,[30] research on STMDs in footbridges typically overlook the impact of this effect.[39,40] Another example is the study by Barrera et al.,[41] which investigates the performance of a STMD on a FRP pedestrian structure. However, the results presented for the optimization of the STMD and TMD are not elaborately detailed and align with the findings of Soria et al.[42] This suggests a need for further research to achieve a more comprehensive understanding of the operational characteristics and performance parameters of STMDs.

This study introduces a comprehensive HSI model in which each pedestrian is considered as an individual degree of freedom. This approach allows for a detailed evaluation of the detuning and uncertainty effects caused by pedestrian-induced vibrations on both TMD and STMD. Furthermore, the STMD studied can adjust

its frequency through damping force, allowing it to respond to nearly instantaneous frequency changes, such as those caused by pedestrian flow in very lightweight structures. Additionally, contour maps are presented to depict the performance and vibration reduction capabilities of these control systems. These maps serve as valuable tools for structural designers, enabling them to assess the impact of HSI on their structures and make informed decisions regarding the implementation of TMDs or STMDs. This is crucial as many design firms currently overlook HSI and vibration control, despite the VLSS often dictating the design of pedestrian bridges.

The paper is organized as follows. Section 2 explains the HSI model used and the vibration inertial control devices studied, which include TMD and STMD. Section 3 explores a sensitivity analysis and Section 4 presents a case study demonstrating the performance of both control strategies applied to a real footbridge considering HSI. In such cases, STMDs (which cover a wider frequency range in the spectrum) can accomodate potential detuning scenarios if they have been wisely tuned initially. Finally, Section 5 contains the main conclusions and key observations from this study.

2. Human-structure interaction and vibration control

2.1. *Human-structure interaction*

Incorporating pedestrians as mass-spring-damper-load systems increases the overall-system's damping ratio, which results beneficial from a vibration control perspective. However, in scenarios with medium to high pedestrian densities, substantial accelerations may still occur.[43] This scenario is especiffically delicate in structures dynamically controlled by TMDs, as the changes on the modal properties of the footbridge due to the influence of HSI, can produce the detuning of the controller regarding its damping effectiveness precisely when it is most required. STMDs, which more effectively cover a wider frequency spectrum, must be tuned to accommodate potential detuning scenarios. Such tuning should consider the likelihood of each scenario and its impact on the structure, particularly focusing on the severity and the maximum RMS acceleration recorded.

The HSI model used in this paper, depicted in Figure 1 is able to capture, in a simple way, changes on the modal parameters of the structure due to the presence of moving humans,[44] that might lead to greater-than-expected detuning of passive inertial controllers.

The HSI model for one pedestrian is mathematically formulated as:

$$m_s\ddot{z}_s + c_s\dot{z}_s + k_s z_s + c_h(\dot{z}_s - \dot{z}_h) + k_h(z_s - z_h) = \phi(vt)F_{ha} \tag{2.1}$$

$$m_h\ddot{z}_h + c_h(\dot{z}_h - \dot{z}_s) + k_h(z_h - z_s) = 0, \tag{2.2}$$

being m_s, k_s and c_s, the generalized mass, stiffness and damping associated to the vibration mode studied, $\phi(vt)$ the mode shape at the position $x = vt$ with v being the walking speed of the pedestrian, t the time and z_s and z_h the vertical

output

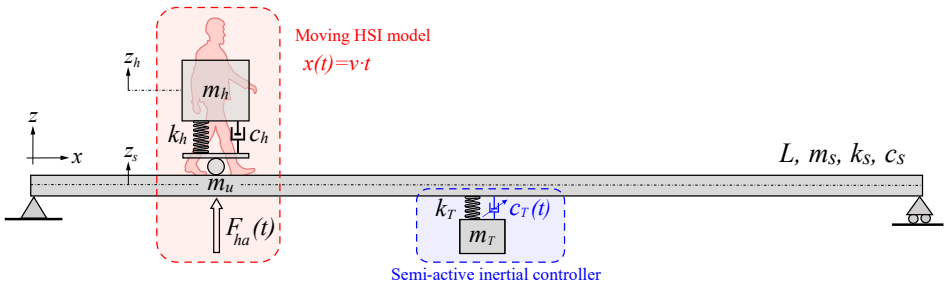

Fig. 1. Structure with a mass-spring-damper pedestrian model and with a semi-active inertial controller. Blue symbol over the controller's dashpot (↗) means changing over time.

displacements of the structure and the pedestrian, respectively (upper dots indicate time derivatives).

The parameters of the human interactive model are calculated from its natural frequency and damping ratio according to: $k_h = \omega_h^2 m_h$ being $\omega_h = 2\pi f_h$ the pedestrian's angular natural frequency and f_h the natural frequency of the human-interactive model and $c_h = 2\omega_h m_h \zeta_h$ with ζ_h being the damping ratio of the model. Rearranging Eqs. (2.1)-(2.2) and extrapolating to a general case with n pedestrians, the CSI model is transformed into a matrix equation, as presented below:

$$\mathbf{M}(t)\ddot{\mathbf{z}}(t) + \mathbf{C}(t)\dot{\mathbf{z}}(t) + \mathbf{K}(t)\mathbf{z}(t) = \mathbf{F}(t). \tag{2.3}$$

The detailed equations of the HSI model, including the equations of motion for the human-bridge-TMD/STMD system, can be found in Appendix A titled "*Detailed equations of the Human-Structure Interaction and control systems*".

The vertical dynamic force exerted by the i^{th} human over the footbridge, $F_{ha,i}(t)$, it is defined as:

$$F_{ha,i}(t) = W_h \sum_{r=1}^{N_r} \mathrm{VDLF}_r \, \sin\left(r\, 2\pi f_{as} t + \varphi_r\right) \quad [\mathrm{N}], \tag{2.4}$$

where W_h is the average of a human (usually taken equal to 700 N), N_r is the total number of harmonics considered, r is the harmonic number, f_{as} is the step frequency, and φ_r is the phase or lag angle of the r-th harmonic. Coefficients referred as Vertical Dynamic Load Factors (VDLFs) are employed in Eq. (2.4) which do not have the same value as the DLFs typically used in non-interacting load models. Eq. 2.3 may be solved employing a direct time integration algorithm, such as the Newmark-beta method.

The model described earlier is described in detail in a contribution by Jimenez-Alonso et al.[13] in which establishes the mean parameters as well as the associated deviation to account for uncertainty in the characteristics of each pedestrian during pedestrian stream. The parameters of the human interactive model (see Figure 1) reported by Jiménez-Alonso et al.[13] are employed in this paper: $f_h = \mathcal{N}(2.93,\, 0.0728)$ Hz, $m_h = \mathcal{N}(0.87,\, 0.048) \cdot m$ kg with m being the total mass

of the pedestrian (the other part is unprung mass, m_u) and $\zeta_h = \mathcal{N}(0.41, 0.047)\%$. The force coefficient for the first harmonic is $\text{VDLF}_1 = \mathcal{N}(0.237, 0.04)$ and $\text{VDLF}_2 = \mathcal{N}(0.043, 0.004)$ for the second.[13] The synchronization angle between pedestrians or interpedestrian synchronization, φ_r, considered in the applied force F_{ha} of each individual is defined by a Poisson distribution with $\lambda = 1$. The step frequency, f_{as}, is adopted as a normal distribution $\mathcal{N}(1.87, 0.175)$ Hz.[3] A total of 500 simulations were conducted for different pedestrian densities, varying the linear mass and vibration frequency of footbridges with a 30 m span. This set of simulations will be described in detail later. Within this comprehensive set three scenarios have been assessed: an uncontrolled structure, a structure controlled with a TMD, and a structure controlled with a STMD. In total, the analysis performed encompassed 1 500 cases. In each case, Eq. (2.3) is implemented and solved in MATLAB[45] using the β-Newmark time integration, with $\beta = 1/4$ and $\gamma = 1/2$ to achieve an unconditionally stable solution.[46] In order to ensure both accuracy and stability in the dynamic response of the controlled structure, a detailed sensitivity analysis was performed. This analysis focused on the time increment, leading to the selection of 0.002 seconds as the optimal value that balances solution accuracy with simulation time. The following section discusses the design and implementation of the two inertial control strategies studied in the paper.

2.2. *Vibration control strategies*

Inertial controllers, TMD and STMD, are modeled similarly to a HSI pedestrian model, but without the unsprung mass and with a fixed position. Both the TMD and STMD systems were positioned at the midspan of the footbridge. In addition, they adopt specific tuning parameters for each case. Further equations are not included in this paper, as the controller model is a simplified version of the HSI model for a pedestrian, which has been addressed earlier.

2.2.1. *Passive control: Tuned Mass Damper*

A TMD consists of a secondary mass (also called moving or inertial mass) attached to the structure using springs and dampers. The TMD moving mass is designed as a fraction of the modal mass of the unique targeted vibration mode; the stiffness of the springs is selected to obtain an optimum TMD tuning frequency. The viscous damper not only ensures energy dissipation but also provides robustness against detuning, allowing for effective performance over a range of frequencies around the tuning frequency. However, TMDs usually have a relatively poor performance for low-level vibrations (as the dry friction of the damper prevents its activation in these cases) and also they still exhibit a significant lack of performance if detunning occurs.

Figure 1 shows the model of a classical TMD composed of an inertial mass $m_{_T}$ attached to a primary system by means of a spring of constant $k_{_T}$ and a viscous damper of constant $c_{_T}$. In Figure 1 it has been highlighted that $c_{_T}(t)$ may vary

output

in real-time. In such case the inertial controller would be a SMTD. The primary structural system to which the controller is attached has been modelled with an equivalent SDOF with the same natural frequency and damping ratio as those of the vibration mode studied. This SDOF has a mass $m_{_S}$, a spring constant $k_{_S}$ and a viscous damper of $c_{_S}$.

The TMD has been designed using the approximate solution provided by Asami and Nishihara,[47] based on H_∞ optimization for primary systems with vanishing damping. The expressions by Asami and Nishihara[47] minimize the maximum stationary acceleration which is related with potential applications in footbridges and also to assess the pedestrian comfort. The TMD properties when the primary system acceleration under harmonic excitation is minimized are:

$$\eta = \sqrt{\frac{1}{1+\mu}} \tag{2.5}$$

$$\zeta_{\mathrm{T}} = \sqrt{\frac{3\mu}{8(1+\mu)^3}} \cdot \sqrt{1+\frac{27}{32}\mu}, \tag{2.6}$$

in which $\mu = m_{_T}/m_{_S}$ is the mass ratio, $\eta = \omega_{_T}/\omega_{_S}$ is the frequency ratio and the stiffness and damping coefficient for the TMD are obtained from:

$$k_{_T} = \omega_{_T}^2 m_{_T} \tag{2.7}$$

$$c_{_T} = 2\zeta_{_T} m_{_T} \omega_{_T}, \tag{2.8}$$

respectively.

2.2.2. *Semi-active Tuned Mass Damper*

A phase control strategy for the STMD damping is considered here. The phase control presented in[25,48] and adapted by Moutinho[49] has been adopted since this is clearly geared to practical implementation due to the measured real-time parameters employed: the structure acceleration, $\ddot{z}_{_S}$, instead of displacement and the inertial mass velocity, $\dot{z}_{_T}$, instead of the relative velocity. This control law will then be effective when the structure's velocity is negligible with respect to the velocity of the inertial mass (something which usually happens in civil engineering structures at resonant response, as the controller usually moves more intensly than the structure). The lowest structural response is achieved when the velocity of the inertial mass and structure's acceleration have opposite phases, so the semi-active device objective is to bring the inertial mass motion as close as possible to this phase. This is equivalent to a phase lag of 90º between the structure acceleration and the control force (porportional to the moving mass acceleration). The control law adopted is of the ON/OFF type due to its simplicity. Thus, the adopted control law when ideal viscous damping is assumed is defined as:

$$\begin{cases} \ddot{z}_{_S} \cdot \dot{z}_{_T} \leq 0 & \Rightarrow \quad c_{_T} = c_{\min} \quad \text{(normal functioning)} \\ \ddot{z}_{_S} \cdot \dot{z}_{_T} > 0 & \Rightarrow \quad c_{_T} = c_{\max} \quad \text{(blocked functioning)}, \end{cases} \tag{2.9}$$

where the maximum damping achieved by the damper is denoted by $c_{\max}$ and the minimum damping by $c_{\min}$. The $c_{\min}$ and $c_{\max}$ used in the semi-active ON/OFF law have been chosen $c_{\max} = 40 \cdot c_T$ and $c_{\min} = c_T/3$ based on the results obtained by Soria et al.[42] The STMD's frequency is also tuned according to the Asami-Nishihara formula,[47] similarly to the TMD. The integration of the STMD into the dynamic model is similar to the one of the TMD, but implementing the control law to vary the parameter $c_{_T}$ with time. Lastly, the semi-active control law includes a trigger based on a minimum running RMS acceleration value, allowing the semi-active control to connect or disconnect during periods of inactivity or very low dynamic response.

3. Sensitivity analysis

While pedestrian stream can trigger various vibration modes,[43] the most significant acceleration amplitudes occur when resonance is reached in a critical mode, often when assessing medium span footbridges. This fact suggests focusing on a single vibration mode for the analysis, as it is likely to experience resonance and generate the most substantial dynamic response. This decision also reduces the computational cost of the model solved.

The authors have decided to focus on pedestrian stream dynamic loading cases as these situations are the more susceptible to cause excessive vertical accelerations. Various pedestrian stream densities have been studied, including 0.1, 0.2, 0.5, 1.0, 1.2, and 1.5 P/m^2, with P/m^2 referring to pedestrians per square meter. These pedestrian streams have been simulated on a simply supported pedestrian bridge with a span of 30 m and a width of 1 m. A graphical description of each simulation has been provided in Figure 2. Before running the analysis, the pedestrians are placed over an approximation path that extends over 1.5 times the length of the footbridge ($30 \cdot 1.5 = 45$ m). This initial disposition is configured to ensure a given pedestrian density over the footbridge. Then, the simulation begins and each pedestrian starts walking with particularized pacing properties. In each simulation, there is a sufficiently long period during which the entire footbridge is loaded by pedestrians. Each simulation finishes when all the pedestrians have abandoned the footbridge, thus, the duration of each simulation was set to allow the entire stream to pass over the structure. This methodology ensured that for 15 m and one-third of the simulation time, the stream density was consistently maintained. Streams of greater length were not studied due to computational constraints, as the increase in computation time grew exponentially with both the number of pedestrians and the simulation duration.

The fundamental natural frequency of the bridge and its associated generalized modal mass are varied by changing distributed mass per linear meter of the structure. frequencies studied in the paper range from 1 Hz to 5 Hz, based on the resonance risk ranges outlined in the Setrá guide,[3] shown in Table 1. The linear mass has been varied from 200 kg/m (which corresponds to an ultra-lightweight

output

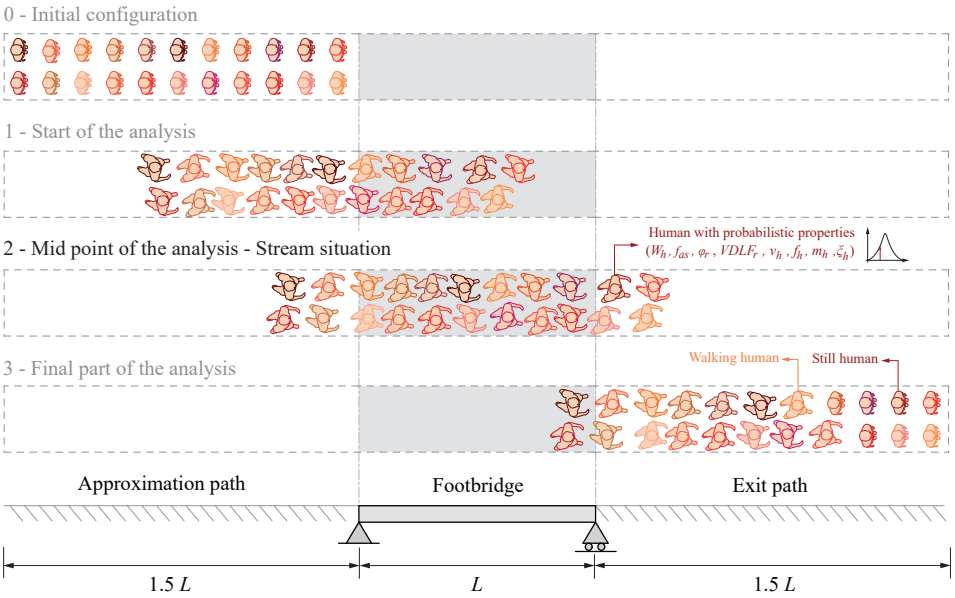

Fig. 2. Simulation explanation. Different phases of the analysis

steel or composite material footbridge) to 2 000 kg/m (typical of much heavier concrete footbriges). Notably, the modal mass represents half the total mass of a simply supported beam, thus this is equivalent to varying the modal mass from 3 000 to 30 000 kg and from 100 to 500 the modal mass / (span · width) ratio. The reasoning for this ratio is to ensure that the results of the sensitivity analysis and contour plots can be extrapolated to different footbridges with varying linear mass, span, and width values. These results, presented as abacuses, can be valuable tools for structural designers, helping them evaluate comfort levels and the need to consider HSI effects.

Table 1 shows frequency ranges classified by resonance risk for vertical vibration due to pedestrian traffic according to Setrá[3] to comply the VSLS.

Table 1. Frequency range classification according to Setrá[3] for vertical vibration.

	Frequency [Hz]					
Resonance risk	0 – 1	1 – 1.7	1.7 – 2.1	2.1 – 2.6	2.6 – 5	> 5
Maximum						
Medium						
Low						
Negligible						
	1 Hz				5 Hz	

Table 2 presents a summary of the varied structural parameters, along with the mass ratio used for the TMD and STMD, which was set at 2% for all the simulations carried out. This mass ratio was selected because it is a commonly adopted value in practice and the study focuses on the robustness of the control devices against detuning due to pedestrian flow rather than on evaluating the comfort level provided.

Each combination of parameters results in a specific structural configuration, and both TMD and STMD are tuned according to the equations described above. The only constant element across all cases is the characteristics of the pedestrian stream, which, despite inherent uncertainty, remains consistent throughout the study.

Table 2. Sensitivity analysis' parameters.

Parameter	Value / Range
Span, L [m]	30
Width, [m]	1
Modal mass, m_S [kg]	3000 – 30 000
Linear mass, [kg]	200 – 20 000
Damping ratio, ζ_S [%]	0.5
Frequency, f_S [Hz]	1.0 – 5.0
Mass ratio, μ	0.02

As noted in the Introduction, the comparison between HSI and moving point loads has been extensively studied, so this topic is not part of this paper. Previous research has also explored the use of passive and adaptive TMD in the context of HSI. This study examines whether STMD can enhance vibration control when considering HSI effects. The sensitivity analysis focuses on varying the modal mass and natural frequency of the structure, while keeping the pedestrian stream parameters constant.

3.1. *Uncontrolled response*

Acceleration results are shown in Figure 3 and have been obtained for the structure without any control mechanisms applied. Notably, this figure reveals that the influence of the second pedestrian harmonic is significant only for lower linear masses and is more pronounced at an intermediate pedestrian stream of 1 P/m^2. The figure confirms that streams with a medium-high pedestrian density are those reaching higher resonant accelerations, as could be expected. On the one hand, when pedestrian density is low, the total human-induced load is low, and thus, the response is limited. On the other hand, when the pedestrian density is high, the modal damping of the footbridge and its mass increases significantly limiting the response. At medium pedestrian densities, the dynamic load is high enough and the damping increase is yet scarce, which provides a maximum response. This effect has been experimentally observed by several authors.[43]

output

Additionally, it is curious to observe that for ultra-lightweight footbridges, the higher the pedestrian density, the higher the natural frequency of the bare structure at which the acceleration is maximum.

3.2. *Controlled response*

Each one of the contour plots above presented can be transformed into a cummulative distributed function (CDF) curves, by rearranging all the points that conform the contour surface in terms of the acceleration and the percentage of non-surpass of that acceleration. This procedure allows data originally expressed in two dimensions to be visualised in a one-dimensional graph and it facilitates easier comparison between the results of the uncontrolled case and those of the controlled cases involving TMD or STMD.

Figure 4 displays the CDF curves for peak acceleration across various pedestrian stream rates. These curves are plotted for the uncontrolled structure, as well as when it is controlled with TMD and STMD.

Although it is useful to represent each scenario with its respective pedestrian stream rates, a more valuable perspective comes from comparing the uncontrolled case with those controlled by TMD and STMD across the same streams. This comparison is shown in Figure 5. Both control methods achieve a greater reduction in acceleration amplitudes above 0.1 m/s^2 compared to the uncontrolled case, especially at lower pedestrian streams. This evidences the better adaptiveness shown by the STMD when detuning occurs. This enhanced reduction of the STMD is especially significative at the peak accelerations of cases with high-medium pedestrian densities.

Contour plots are used again to compare the cases controlled by TMD and STMD in Figure 6. This figure has been conceived as a table of subfigures, where each row corresponds to a given pedestrian density (0.1, 0.5, 1.0 and 1.5 P/m^2) and each column represents a type of controller used (TMD at left and STMD at right). Each subfigure represents a contour plot of the vibration reduction achieved by each controller. A significant observation from these plots is that the STMD demonstrates superior performance compared to the TMD, particularly evident curves with smaller CDF areas (Figures 4 and 5) and in the higher vibration reduction percentages indicated by the darker shades on the contour plots (Figure 6), both when resonance occurs with the first pedestrian harmonic and the second pedestrian harmonic. However, in cases with an extremely low structural mass, both inertial control devices exhibit reduced effectiveness due to an insufficient mass ratio between the inertial control devices and the pedestrian mass. In addition, the response becomes less resonant, becoming more transient and involving more modes of vibration.

To better compare these contour plots illustrating vibration reduction by TMD and STMD, CDF curves are used again in Figure 7. These curves reveal that the STMD matches or outperforms the TMD in terms of acceleration distribution in

output

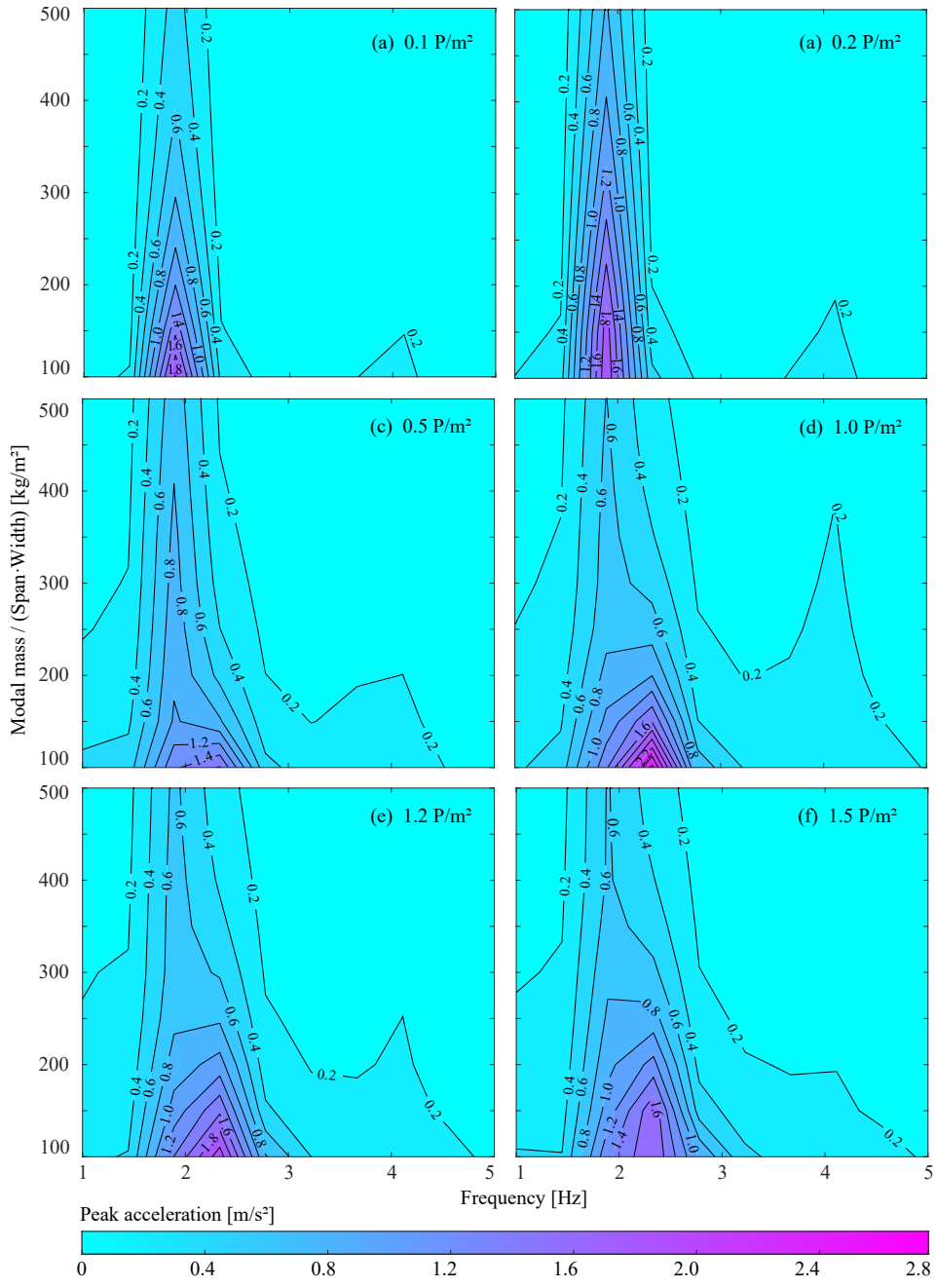

Fig. 3. Contour plots for peak acceleration of pedestrian streams for uncontrolled structure

output

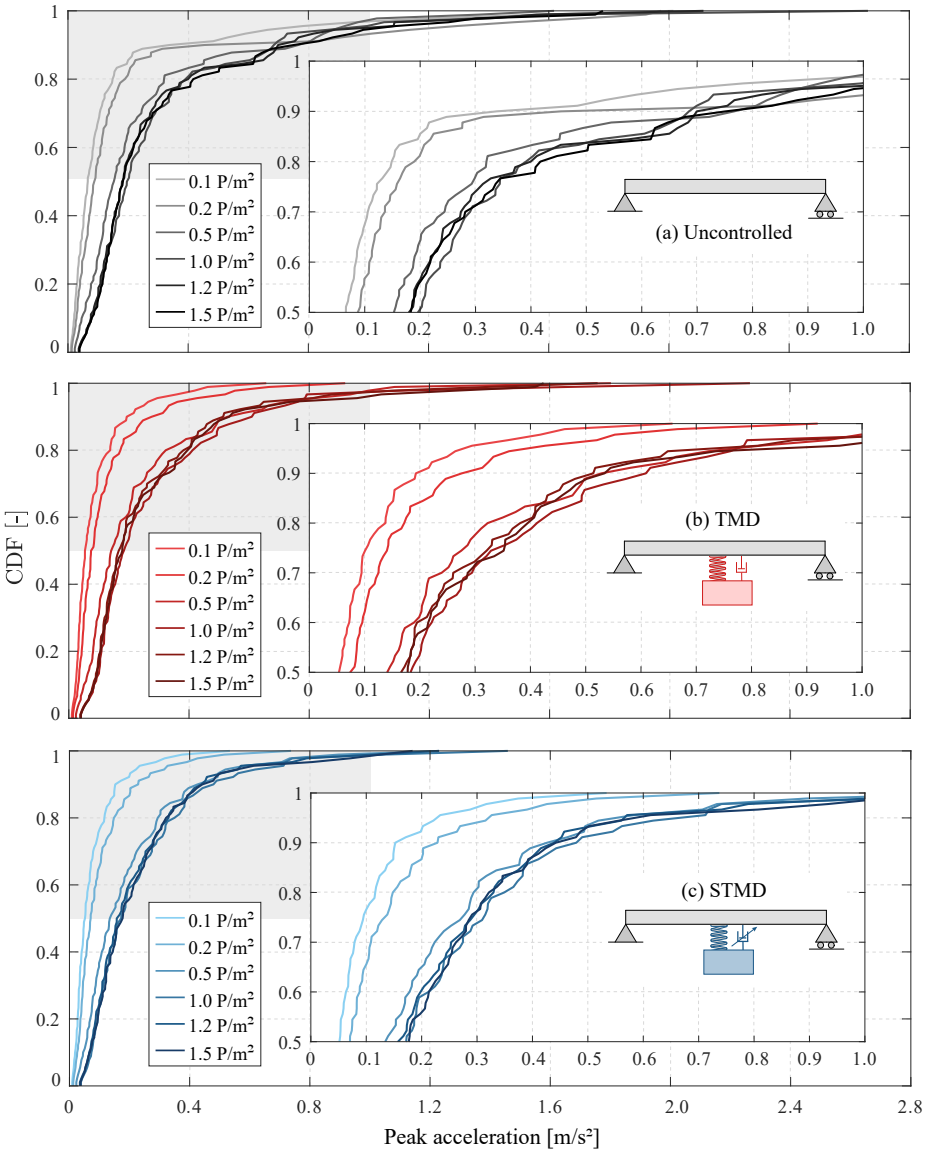

Fig. 4. CDF curves for the peak acceleration for different pedestrian stream values.

almost all cases. Both devices achieve greater reductions with lower pedestrian stream rates (0.1 and 0.2 $\mathrm{P/m^2}$), and although the reduction decreases as pedestrian density increase. In other words, the TMD performance is considerably degraded by the influence of HSI, while the STMD copes better with this detunning.

To sum up, all vibration reduction curves for TMD and STMD are plotted

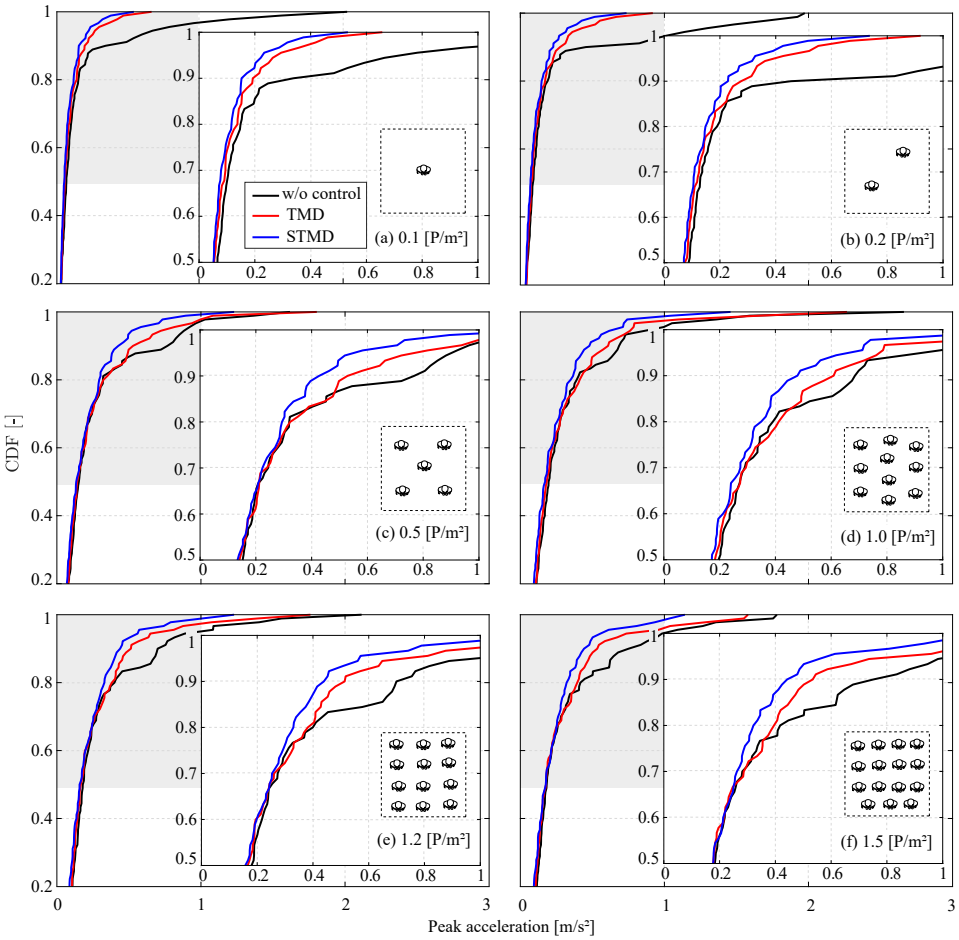

Fig. 5. Comparison of CDF curves for the peak acceleration of pedestrian stream values.

for the different pedestrian stream rates examined in Figure 8. The corresponding envelope polygons of all the TMD and STMD curves have been shaded in this figure with transparent red and blue areas, respectively. The superiority of STMD over TMD is apparent, as it has a smaller area, indicating less dispersion in its results, and a lower, more right-shifted centroid. This suggests improved control in terms of vibration reduction. The properties of the envelope polygons are as follows: passive area (11.22), semi-active area (10.86), passive centroid (34.84, 0.85), and semi-active centroid (36.68, 0.77).

output

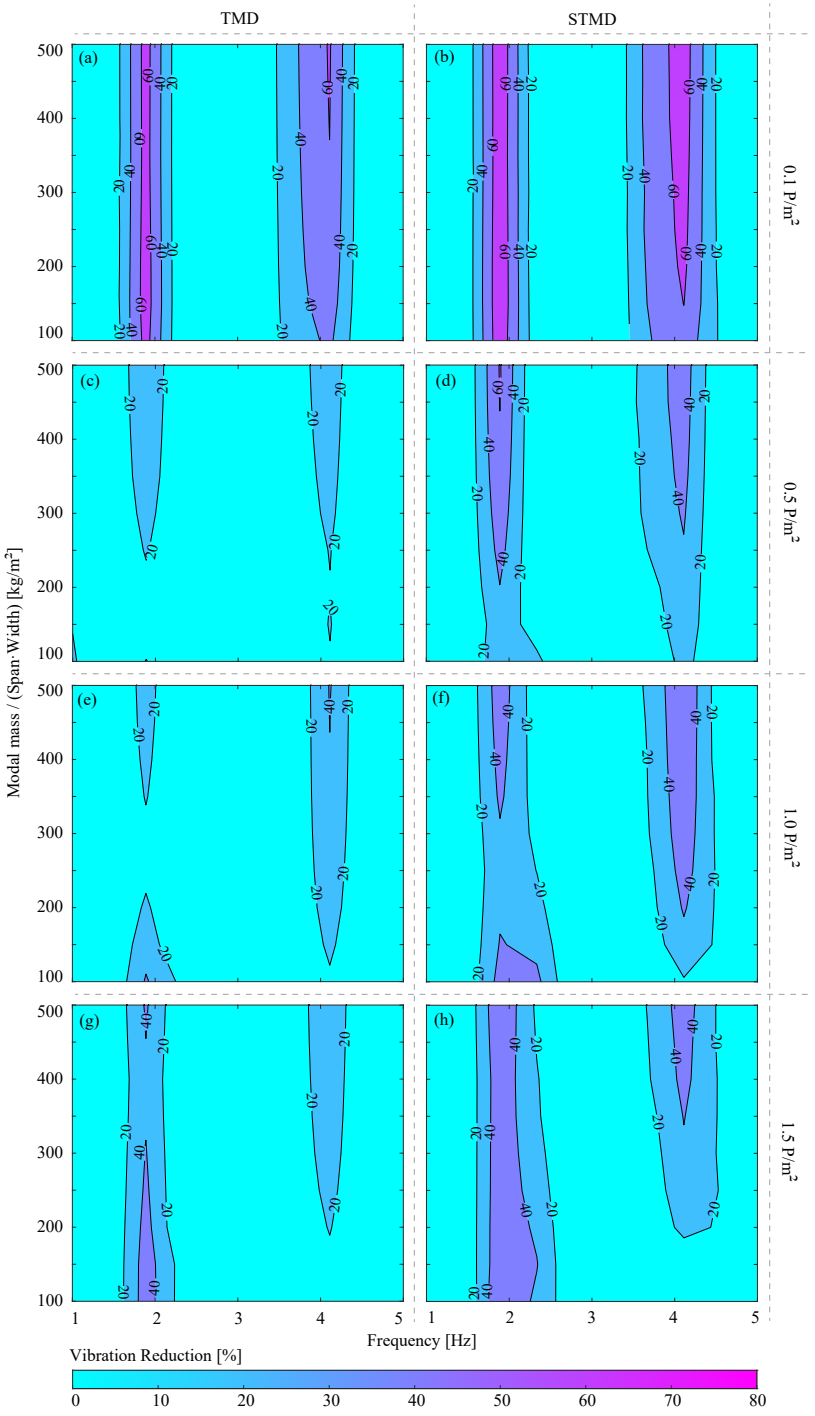

Fig. 6. Contour plots for vibration reduction [%] for TMD and STMD

output

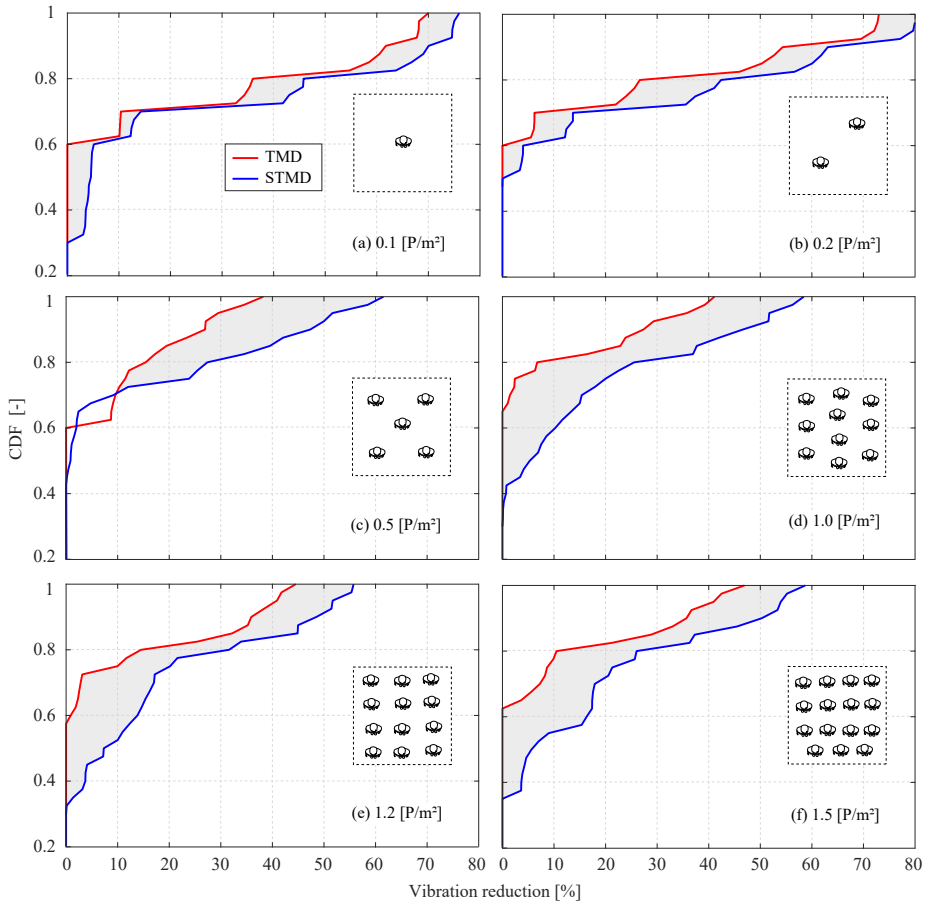

Fig. 7. CDF curves for the vibration reduction (%) of pedestrian stream values.

4. Case study: veterinary faculty footbridge

4.1. *Structure description and its monitoring*

The footbridge examined in this study is a cable-stayed structure with a steel box-girder, located in northwest Madrid, Spain. The structure spans across the A6 highway, connecting the Veterinary Faculty with the main university campus in Moncloa, earning it the name veterinary faculty footbridge. The deck is 45 meters long and 1.5 meters wide. It is supported by a reinforced-concrete pylon through two steel cables at a point 18 meters from the start of the footbridge (see Figure 9(a)). The pylon stands 18 meters tall, and its connection to the girder is rigid. The opposite end of the girder is simply supported at two points: one at the very end and the other 2.8 meters before the pylon, providing additional rigidity. The bridge has a mass per unit length of about 1 000 kg/m, which is an intermediate value among

output

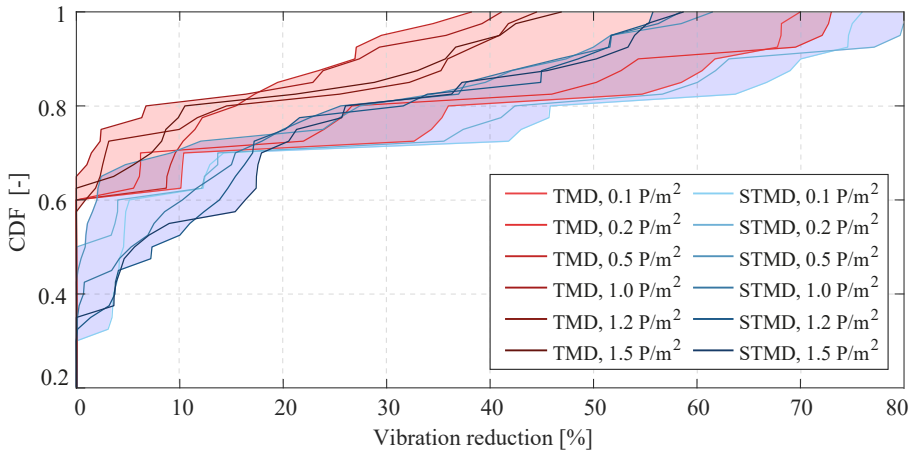

Fig. 8. Summarize of CDF curves.

those explored in previous sensitivity analyses, indicating that this configuration represents a relevant and typical case for study. The estimated generalized modal mass is 21 859 kg. This value accounts for about 49% of the total mass of the footbridge, indicating that it behaves similarly to a simply supported structure. This structure has a modal mass / (span · width) ratio of 366.66 kg/m^2, its 1.5-meter width allows for two pedestrians to walk side by side along the same longitudinal coordinate.

(a) South view for the A6 highway.

(b) Wireless accelerometer.

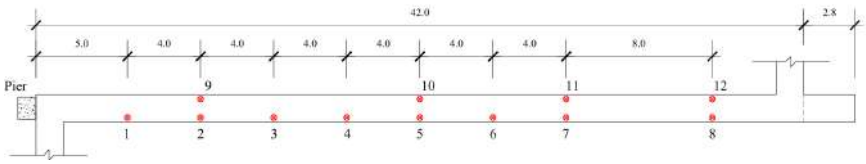

(c) Setup configuration plan. Dimensions in m

Fig. 9. Veterinary faculty footbridge.

The ambient vibration test took place in May 2022. For the test, 12 measurement points were established along the footbridge's length (as shown in Figure 9(c)), deemed sufficient to identify the first three vertical vibration modes. Acceleration data was collected using four wireless accelerometers (MR3003C, Syscom Instruments), depicted in Figure 9(b). One accelerometer was kept in a fixed location (reference accelerometer, point 6 in Figure 9(c)), while the other three were moved to different positions in each setup. In total, four setups were performed, each lasting 600 seconds with a sampling frequency of 2 000 Hz. The data was preprocessed with a low-pass filter with a cutoff frequency of 20 Hz and a signal decimation by a factor of 50. The measurements were then analyzed in the time domain using the covariance-driven Stochastic Subspace Identification algorithm.[50] Figure 10 shows the first three estimated vertical vibration modes for the cable-stayed bridge.

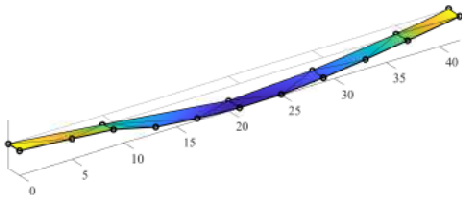

(a) Mode 1 ($f_1 = 1.81\,\text{Hz}$, $\zeta_1 = 0.81\%$).

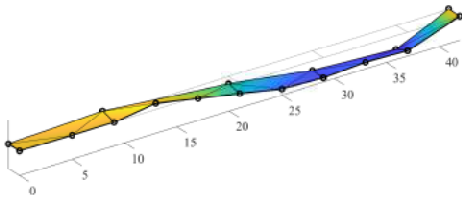

(b) Mode 2 ($f_2 = 5.97\,\text{Hz}$, $\zeta_2 = 0.74\%$).

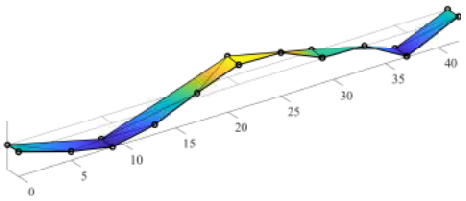

(c) Mode 3 ($f_3 = 10.53\,\text{Hz}$, $\zeta_3 = 0.80\%$).

Fig. 10. First three vertical modal shapes of the vibration modes of the structure obtained from the experimental campaign.

Despite the HSI model being previously validated in Jimenez-Alonso,[13] a separate test involving groups of 6 pedestrian walking synchronously at 1.81 Hz pacing frequency was conducted (see Figure 11(a) and (b)), with results closely mirroring those obtained through the HSI model (see Figure 11(c)). To simulate the dynamic response of the structure subjected to this group of pedestrians, the HSI model was employed. The following constitutive parameters were considered: (i) for the pedestrian model, parameters provided by Jimenez-Alonso[13] were used, and (ii) for the structural model, an equivalent single degree of freedom model, as recommended by SYNPEX guidelines,[51] was utilized. The natural frequency and associated damping ratio of this numerical model were based on the first experimental vibration

output

modes. Additionally, the modal shape of this model was approximated using a sinusoidal function. In the specific case of the simulations shown in Figure 11(c), the HSI model described in the article was used with the following modifications: the pedestrians walked with a deterministic step frequency, directly related to their walking velocity, that matched the structure's vibration frequency, rather than a normally distributed step frequency. A group of pedestrians differs from a pedestrian stream, in that in a group all the pedestrians walk close together, rather than spread out along the footbridge. Thus, the phase shift variable for their steps, or the inter-pedestrian synchronization, was set to zero, ensuring perfect synchronization among the pedestrians. Apart from the step frequency and synchronization angle, all other variables (pedestrian mass, frequency, and damping distributions) were set to the mean values of their respective distributions, consistent with those used in the HSI model described by Jimenez-Alonso.[13] This initial comparison aimed to confirm the reliability of the HSI model for this specific structure. Later, a subsequent set of results has been obtained to compare the performance of both control strategies if applied to this particular structure, considering the influence of the previously validated HSI model. For this second analysis, unsynchronized free pedestrian stream loading cases have been considered. This choice was made because the primary objective of this study is to evaluate the performance of TMD and STMD for vibration control, with the consideration of HSI in a broader structural context. For numerical analysis of the uncontrolled structure, TMD-controlled structure, and STMD-controlled structure, modal parameters from the first mode of vibration were used to ensure consistent assessment across cases.

4.2. *Performance of the control strategies*

In this subsection, the dynamic performance of a TMD and a STMD with a mass ratio of 2% has been studied for this particular structure as a function of the pedestrian density of an unsynchronized stream loading case and using the modelling methodology above described for considering the HSI. The optimal parameters of the controllers have been designed according to Asami and Nishihara formulae.[47] Both the TMD and STMD systems are configured with a stiffness value of $k_T = 5.435e04$ N/m. In addition, damping coefficients were determined as follows: i) for the TMD system: $c_T = 835.948$ N·s/m; and ii) for the STMD system: $c_{\max} = 40 \cdot c_T = 3.344e04$ N·s/m and $c_{\min} = c_T/3 = 278.649$ N·s/m.

In this study, the results of the structural response obtained considering HSI have been compared with a second set of simulations in which HSI has not been considered. Thus, the pedestrian loading is considered just as an external load, not as an interactive system. This second set of structural responses has been computed using the provisions given by the guidelines SÉTRA[3] and HIVoSS.[5] The authors consider that the methodology proposed by these documents serves as a standard for comparison. Their approach starts by considering the footbridge as the equivalent SDOF system of its critical mode of vibration, in this case, the fundamental one,

output

(a) Lateral view. (b) Longitudinal view.

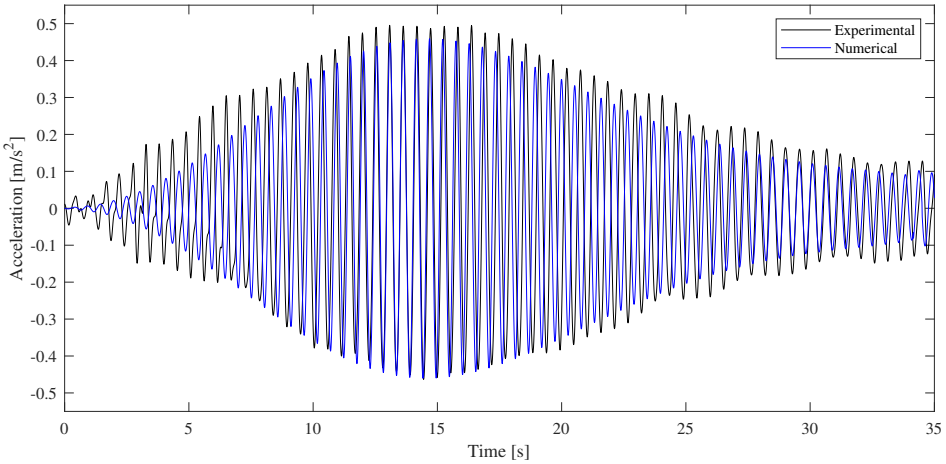

(c) Comparison between experimental and numerical results.

Fig. 11. Experimental tests of a group of 6 walking pedestrians synchronized to the resonant frequency of the structure.

with a mass equal to 21859 kg, a natural frequency equal to 1.81 Hz and a damping ratio equal to 0.81%. The vertical load of a stream of pedestrians is modelled as a uniformly distributed sinusoidal load in resonance with the critical mode and in phase with it. The amplitude of this load depends on the pedestrians' density, the dimensions of the footbridge, its natural frequency and its damping ratio. To work with the equivalent SDOF of the structure, an equivalent load of the pedestrian stream needs to be computed. This is done by integrating the product of this load by the fundamental mode of vibration along the whole length of the footbridge. Finally, the controllers are attached to the equivalent SDOF of the footbridge as

output

before. For each analysis, the stream load has been applied during 70 seconds and the steady-state peak acceleration has been obtained.

The results obtained for the two sets of simulations have been depicted in Figure 12. Figure 12(a) provides the peak acceleration of each case as a function of the pedestrian density. There, the interactive cases are depicted with continuous lines and the non-interactive cases with dashed lines. Figure 12(b) provides a zoom-in of Figure 12(a), to better distinguish the responses of the controlled cases with and without considering HSI. Finally, Figure 12(c) shows the vibration reduction of the TMD and the STMD with respect to the uncontrolled case as a function of the pedestrian density. First of all, in Figure 12(a) it is evident that the uncontrolled response predicted without accounting for HSI is excessive and not realistic (something well-known in the research field). When looking at the uncontrolled response with HSI in Figure 12(b), it can be clearly seen that the maximum acceleration remains approximately constant independently on the pedestrian density of the stream crossing the footbridge. Two, slight peaks can be appreciated, one ocurring at a density of 0.18 P/m^2 and the other at 1.38 P/m^2. The graph reveals that in the vertical direction, relatively high amplitudes can be reached even with low numbers of pedestrians, unlike in the lateral direction, where the "lock-in" phenomenon requires sufficient pedestrian density, amplitude of acceleration, and being within a critical frequency range. Diving into the controlled responses, it can be seen that they are similar whether or not HSI is considered. However, the vibration reduction they provide with respect to the uncontrolled decreases substantially when HSI is accounted for, as can be appreciated in Figure 12(c). These two aspects evidence that the HSI increases substantially the damping of the footbridge, thus reducing the effectiveness of the the control devices, and especially of the TMD. Another interesting element from Figure 12(c) is that the stronger higher the influence of the HSI, the higher the difference between the effectiveness of the STMD and the TMD. Overall, STMD consistently outperforms the TMD.

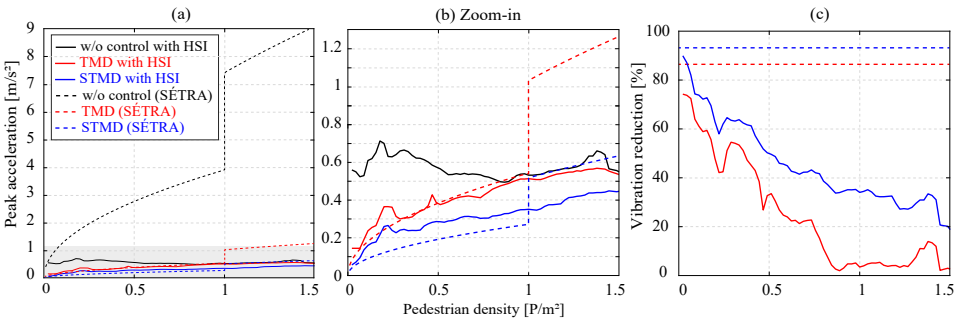

Fig. 12. Veterinarian's footbridge response for different pedestrian stream values.

The analysis demonstrates that both TMDs and STMDs facilitate a gradual

improvement in performance, effectively limiting the amplification for lower pedestrian densities. However, it is crucial to note that the vibration reduction achieved by the TMDs becomes significantly less effective for pedestrian densities exceeding 0.85 P/m^2. In contrast, STMDs maintain a vibration reduction that exceeds 20% even at higher pedestrian densities, up to 1.5 P/m^2. The maximum observed reduction difference is 32%, occurring at a pedestrian density of 0.89 P/m^2, while the minimum difference observed is 9%, observed at a density of 0.29 P/m^2.

Again, CDF function are used to analyse the effectiveness of the controllers. Figure 13(a) shows the CDF for the peak acceleration for each case, and Figure 13(b) the CDF of the vibration reduction for each controller. Figure 13 shows the CDF curves of peak acceleration and vibration reduction to evaluate performance of both. The area between the CDF curve and the y-axis provides an indication of performance for both acceleration and vibration reduction. When assessing accelerations, a CDF curve that shifts further to the right indicates more area and therefore a worse performance, signifying higher acceleration amplitudes. For vibration reduction, a curve that moves to the right indicates a larger area and improved performance, showing greater vibration reduction. The CDF area values for acceleration are 0.72 for the uncontrolled case, 0.54 for the TMD case, and 0.38 for the STMD case. This indicates that both TMD and STMD reduce acceleration amplitudes, with STMD showing the greatest improvement. For vibration reduction, the area values are 0.24 for TMD and 0.44 for STMD, highlighting that STMD provides significantly better vibration reduction compared to TMD.

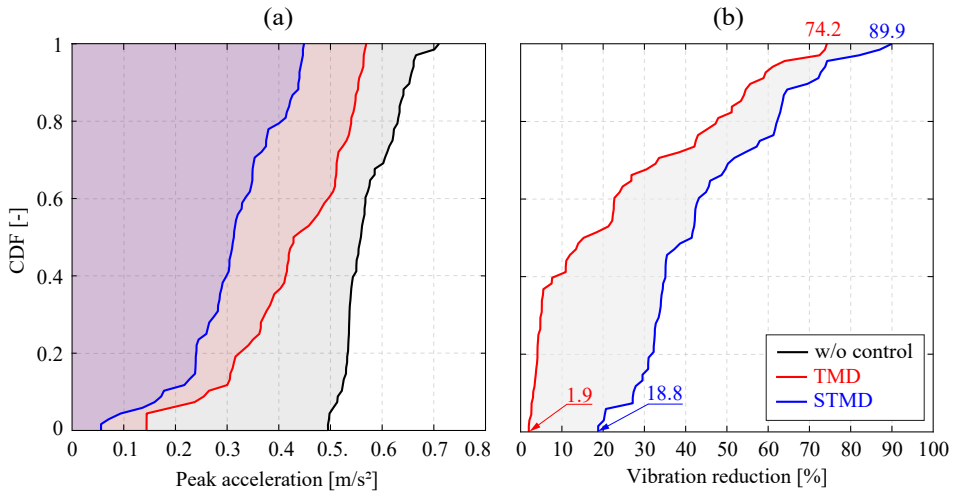

Fig. 13. CDF curves of Veterinarian's footbridge response.

output

5. Conclusions

This paper has studied the impact of HSI on the dynamic behavior of footbridges and its influence in the vibration cancellation performance of two types of inertial controllers, TMDs and STMDs. The impact of HSI extends beyond merely augmenting structural damping and reducing vibration amplitudes; since it tends to modify and to introduce variablity in the modal parameters of the structure. This variability enhances the efficacy of STMDs, which can adjust their damping properties in real-time, thus maintaining effective control over a range of frequencies. This adjustment allows the STMD to operate effectively even when the structure's natural frequency varies due to HSI. In contrast, TMDs have a functioning severely degraded due to detuning issues directly derived from the HSI. This paper has studied these topics through firstly developing a sensibility analysis in which the dynamic response of different 30 m long footbridges with varying massess and fundamental frequencies have been studied for diverse pedestrian stream loading cases. 3 different scenarios have been addressed: the uncontrolled structure, the structure with a TMD and the structure with a STMD. After this initial study a particular case of study of a real footbridge has been carried out. Again, for this particular structure the same 3 scenarios have been explored considering stream loading cases with different pedestrians densities. Thus, a cable-stayed steel box girder bridge of 45 meters long located at the northwest of Madrid has been considered as the case study.

From these two studies the following conclusions can be outlined:

- First of all, from the sensitivity analysis, it can be appreciated that the lower the mass of the footbridge and the higher the pedestrian density of the stream, the more pronounced is the influence of the HIS. In Figure 3, for example, for ultra-lightweight footbridges (the lower band of each contour plot) the frequency of the bare structure at which the acceleration is maximum increases with the pedestrian density. Thus, for low-density cases, this frequency is around 1.8-1.9 Hz while for medium-high-density ones (especially over 0.2 P/m^2), this frequency raises up to values of around 2.2 or 2.3 Hz (increasing around a 20%). This effect is not so pronounced in heavier footbridges (the upper band of each contour plot) where this frequency tends to remain constant. Both facts evidence a significant change in the natural frequency of footbridges when HIS effects are remarkable.

- From this first analysis it can be stablished that a reasonable mass limit under which HSI effects should be considered could be 800 kg/m^2. Furthermore, a pedestrian density of around 0.2 P/m^2 could be considered as lower limit over which HSI should be taken into account.

- This study has proven that the influence of HSI significantly alters the modal properties of lightweight structures. This variability degrades the vibration cancellation performance of TMDs that tend to suffer from detuning issues. For example, From Figure 7 it can be seen how the maximum vibration reduction of TMDs is degraded from 70-75% for low-density cases (when HSI influence is low) till values of around 40-45% for medium-high density cases (where HSI plays an important role). Moreover, looking at the results of the Veterinary Faculty footbridge in Figure 12(b), it can be seen how the vibration reduction of the TMD decreases from 75% till almost 5% from low to higher pedestrian densities.

- On the counterpart, STMDs have proven to have a superior adaptability and effectiveness in this context when compared to TMDs. Their vibration reduction also decreases due to the influence of HSI, but at a lower level than TMDs. In Figure 7 their maximum vibration reduction is degraded form almost 90-100% to 55-60%. In the Veterinary Faculty footbridge, the vibration reduction decreases form 90% till around 20% for high-density cases. These results show that the vibration reduction of STMDs is, in average, a 20% higher than the one of TMDs when HSI is significant (even becoming a 30-35% superior in some cases).

This research has shown how HSI impacts on the dynamic response of footbridges and on the cancelation performance of inertial vibration controllers applied to them. Future research should be focused on the transient response involving multiple vibration modes, as well as on structures with natural frequencies higher than 5 Hz, as lightweight timber building floors. Moreover, a more detailed characterization of the VLDF for the human interactive model is needed. The natural frequencies and damping values for the coupled systems were not dynamically estimated in this study. Future research should focus on dynamically estimating the natural frequencies and damping ratios of the bridge considering HSI for each pedestrian flow density. This would provide a more comprehensive understanding of the dynamics involved and a more accurate tuning of TMD and STMD devices in real-time applications. Refer to Jiménez-Alonso et al.[13] for an example of the impact of pedestrian flow on the natural frequencies of footbridges. Finally, future research related to the wise calibration of TMDs and STMDs applied to footbridges susceptible to experience HSI is needed.

Acknowledgments

The authors acknowledge the grant PID2021-127627OB-I00 (Transport Infrastructures subjected to dynamic loading: assessment techniques for the sustainability, intelligent maintenance and comfort) funded by Ministerio de Ciencia e Innovación, Agencia Estatal de Investigación and 10.13039/501100011033 FEDER, European

output

Union. Christian Gallegos-Calderón expresses his gratitude to the SENESCYT-Ecuador for the financial support.

Appendix A. Detailed equations of the Human-Structure Interaction and control systems

In this appendix, the detailed mathematical formulation of the HSI model is presented, including the equations of motion for the human-bridge and human-bridge-TMD/STMD systems. These comprehensive equations provide a thorough understanding of the interaction mechanisms and the control strategies implemented in the study.

The following equations describe the HSI model coupled with the footbridge, illustrating the interaction dynamics without additional damping devices:

$$\mathbf{M}(t) = \begin{bmatrix} m_s & 0 & \cdots & 0 \\ 0 & m_{h1} & \cdots & 0 \\ & \cdots & \ddots & 0 \\ 0 & 0 & 0 & m_{hn} \end{bmatrix} \tag{A.1}$$

$$\mathbf{C}(t) = \begin{bmatrix} c_s + \phi(vt)_1 c_{h1} \phi^T(vt)_1 + \ldots + \phi(vt)_n c_{hn} \phi^T(vt)_n & -\phi(vt)_1 c_{h1} & \cdots & -\phi(vt)_n c_{hn} \\ -\phi(vt)_1 c_{h1} & c_{h1} & & 0 \\ \cdots & \cdots & 0 & \cdots \\ -\phi(vt)_n c_{hn} & 0 & 0 & c_{hn} \end{bmatrix} \tag{A.2}$$

$$\mathbf{K}(t) = \begin{bmatrix} k_s + \phi(vt)_1 k_{h1} \phi^T(vt)_1 + \ldots + \phi(vt)_n k_{hn} \phi^T(vt)_n & -\phi(vt)_1 k_{h1} & \cdots & -\phi(vt)_n k_{hn} \\ -\phi(vt)_1 k_{h1} & k_{h1} & & 0 \\ \cdots & \cdots & 0 & \cdots \\ -\phi(vt)_n k_{hn} & 0 & 0 & k_{hn} \end{bmatrix} \tag{A.3}$$

$$\mathbf{F}(t) = \begin{bmatrix} \sum_{i=1}^{n} -\phi(vt)_i F_{ha,i} \\ 0 \\ \cdots \\ 0 \end{bmatrix}, \tag{A.4}$$

where $\phi(vt)_i$ refers to the value of the vibration mode of the i-th pedestrian at the position vt. The previous system of equations is expressed for only one vibration mode of the structure. When N_s vibration modes are considered, the order of these matrices is $N_s + n$.

The subsequent equations present the system incorporating the inertial device, TMD or STMD, highlighting the impact of these control devices on the overall system dynamics:

output

$$\mathbf{M}(t) = \begin{bmatrix} m_s & 0 & \cdots & 0 & 0 \\ 0 & m_{h1} & \cdots & 0 & 0 \\ \vdots & \vdots & \ddots & 0 & 0 \\ & & & m_{hn} & 0 \\ 0 & 0 & 0 & 0 & m_T \end{bmatrix} \tag{A.5}$$

$$\mathbf{C}(t) = \begin{bmatrix} c_s + \phi(vt)_1 c_{h1} \phi^T(vt)_1 + \ldots + \phi(vt)_n c_{hn} \phi^T(vt)_n + c_T & -\phi(vt)_1 c_{h1} & \cdots & -\phi(vt)_n c_{hn} & -c_T \\ -\phi(vt)_1 c_{h1} & c_{h1} & & 0 & 0 \\ \cdots & \cdots & \ddots & \cdots & \\ -\phi(vt)_n c_{hn} & 0 & 0 & c_{hn} & 0 \\ -c_T & 0 & 0 & 0 & c_T \end{bmatrix} \tag{A.6}$$

$$\mathbf{K}(t) = \begin{bmatrix} k_s + \phi(vt)_1 k_{h1} \phi^T(vt)_1 + \ldots + \phi(vt)_n k_{hn} \phi^T(vt)_n + k_T & -\phi(vt)_1 k_{h1} & \cdots & -\phi(vt)_n k_{hn} & -k_T \\ -\phi(vt)_1 k_{h1} & k_{h1} & & 0 & 0 \\ \cdots & \cdots & \ddots & \cdots & \\ -\phi(vt)_n k_{hn} & 0 & 0 & k_{hn} & 0 \\ -k_T & 0 & 0 & 0 & k_T \end{bmatrix} \tag{A.7}$$

$$\mathbf{F}(t) = \begin{bmatrix} \sum_{i=1}^{n} -\phi(vt)_i F_{ha,i} \\ 0 \\ \cdots \\ 0 \end{bmatrix}, \tag{A.8}$$

with the difference that their values are different from those of a pedestrian and their position is fixed. Thus, its action is not weighted by the factor $\phi(vt)$ as in the case of pedestrians.

References

1. P. Dallard, A. Fitzpatrick, A. Flint, S. Le Bourva, A. Low, R. Ridsdill and M. Willford, The London Millennium Footbridge, *The Structural Engineer* **79**(22) (2001) 17–33.

2. S. Živanović, A. Pavic and P. Reynolds, Vibration serviceability of footbridges under human-induced excitation: a literature review, *Journal of sound and vibration* **279**(1-2) (2005) 1–74.
3. Technical Department for Transport, Roads and Bridges Engineering and Road Safety, Ministry of Transport and Infrastructure, *SETRA/AFGC. Footbridges – Assessment of vibrational behaviour of footbridges under pedestrian loading*, (2016).
4. ISO 10137, *Bases for Design of Structures – Serviceability of Buildings and Walkways against Vibrations*, international organization for standardization edn., (2007).
5. C. Butz, C. Heinemeyer, A. Keil, M. Schlaich, A. Goldack, S. Trometer, M. Lukić, B. Chabrolin, A. Lemaire, P.-O. Martin, Á. Cunha and E. Caetano, *HIVOSS: Design of footbridges guideline* (Joint Research Center, 2008).
6. CEN, *prEN 1990 Eurocode — Basis of Structural Design; Annex A2/Annex H Verifications Concerning Vibration of Footbridges due to Pedestrian Traffic* (European Committee for Standardisation, oct 2021).
7. CEN, *prEN 1991-2 Eurocode 1 — Actions on structures — Part 2: Traffic Loads on Bridges and Other Civil Engineering Works; Annex G Dynamic Load Models for Footbridges* (Final draft for enquiry. European Committee for Standardization, 2021).
8. A. Tadeu, A. Romero, S. Dias, F. Pedro, M. Brett, M. Serra, P. Galvín and F. Bandeira, Vibration serviceability assessment of the world's longest suspended footbridge in 2020, *Structures* **44** (oct 2022) 457–475.
9. C. Gallegos-Calderón, J. Naranjo-Pérez, J. H. García-Palacios and I. M. Díaz, Design and performance of a tuned vibration absorber for a full-scale lightweight FRP pedestrian structure, *Journal of Composites for Construction* **26**(6) (2022) p. 04022077.
10. P. Dey, A. Sychterz, S. Narasimhan and S. Walbridge, Performance of pedestrian-load models through experimental studies on lightweight aluminum bridges, *Journal of Bridge Engineering* **21**(8) (2016) p. C4015005.
11. C. A. Jones, P. Reynolds and A. Pavic, Vibration serviceability of stadia structures subjected to dynamic crowd loads: A literature review, *Journal of Sound and Vibration* **330** (apr 2011) 1531–1566.
12. E. Shahabpoor, A. Pavic and V. Racic, Interaction between Walking Humans and Structures in Vertical Direction: A Literature Review, *Shock and Vibration* (2016) 1–22.
13. J. F. Jiménez-Alonso, A. Sáez, E. Caetano and F. Magalhães, Vertical crowd–structure interaction model to analyze the change of the modal properties of a footbridge, *Journal of bridge Engineering* **21**(8) (2016) p. C4015004.
14. E. Shahabpoor, A. Pavic and V. Racic, Identification of mass-spring-damper model of walking humans, *Structures* **5** (feb 2016) 233–246.
15. Y. Zhang, W. He, J. Zhang and H. Dong, Experimental and numerical investigation on dynamic properties and human-induced vibrations of an asymmetric steel-plated stress-ribbon footbridge, *Advances in Civil Engineering* (2021).
16. X. Wei, J.-C. Liu and S. Bi, Uncertainty quantification and propagation of crowd behaviour effects on pedestrian-induced vibrations of footbridges, *Mechanical Systems and Signal Processing* **167** (2022) p. 108557.
17. J. M. Soria, J. F. J. Alonso, C. Gallegos, J. Naranjo and C. M. Renedo, Calibration of the dynamic load factor coefficients for third and fourth harmonic for HSI model in an ultra-lightweight frp lab footbridge, in *CMMoST 2021: 6th International Conference on Mechanical Models in Structural Engineering* Universidad de Valladolid, (Valladolid, Spain, 2021).
18. Y. Li, X. Zhang, C. Wang, Y. Zhang and X. Wei, Human-induced vertical vibration of a glass suspension footbridge: experimental study and numerical analysis, *Structure*

and Infrastructure Engineering (2023) 1–19.
19. S. Živanović, I. Díaz and A. Pavić, Influence of walking and standing crowds on structural dynamic properties, in *IMAC XXVII Conference and Exposition on Structural Dynamics* (The Society for Experimental Mechanics, Inc., Orlando, FL, feb 2009).
20. D. Colmenares, G. Costa, M. Civera, C. Surace and R. Karoumi, Quantification of the human–structure interaction effect through full-scale dynamic testing: The Folke Bernadotte bridge, *Structures* **55** (2023) 2249–2265.
21. D. Colmenares, A. Andersson and R. Karoumi, An analytical solution of the maximum response of the coupled multiple parallel modulated pedestrian-bridge system, *Structures* **57** (2023) p. 105160.
22. C. Gallegos-Calderón, C. M. Renedo, M. D. G. Pulido and I. M. Díaz, A frequency-domain procedure to design TMDs for lively pedestrian structures considering Human–Structure Interaction, *Structures* **43** (sep 2022) 1187–1199.
23. F. Ferreira and L. Simões, Least Cost Design of Curved Cable-Stayed Footbridges with Control Devices, *Structures* **19**(November 2018) (2019) 68–83.
24. J. P. Den Hartog, *Mechanical vibrations* (McGraw-Hill, 1956).
25. T. T. Soong and G. F. Dargush, *Passive energy dissipation systems in structural engineering* (John Wiley & Sons, 1997).
26. R. G. Cuevas, J. F. Jiménez-Alonso, F. Martínez and I. M. Díaz, Uncertainty-based approaches for the lateral vibration serviceability assessment of slender footbridges, *Structures* **33** (2021) 3475–3485.
27. M. Fouli and A. Camara, Human-structure interaction effects on lightweight footbridges with tuned mass dampers, **62** (2024) p. 106263.
28. Y. Wang, L. Wang and W. Shi, Two—dimensional air spring based semi—active TMD for vertical and lateral walking and wind-induced vibration control, *Structural Engineering and Mechanics* **80** (nov 2021) p. 390.
29. L. Wang, S. Nagarajaiah, W. Shi and Y. Zhou, Semi-active control of walking-induced vibrations in bridges using adaptive tuned mass damper considering human-structure-interaction, *Engineering Structures* **244** (2021) p. 112743.
30. L. Wang, S. Nagarajaiah, Y. Zhou and W. Shi, Experimental study on adaptive-passive tuned mass damper with variable stiffness for vertical human-induced vibration control, *Engineering Structures* **280** (2023) p. 115714.
31. S. Schleiter and O. Altay, Identification and semi-active control of structures with abrupt stiffness degradations, *Mechanical Systems and Signal Processing* **163** (2022) p. 108131.
32. D. Hrovat, P. Barak and M. Rabins, Semi-active versus passive or active tuned mass dampers for structural control, *Journal of Engineering Mechanics* **109**(3) (1983) 691–705.
33. T. Pinkaew and Y. Fujino, Effectiveness of semi-active tuned mass dampers under harmonic excitation, *Engineering Structures* **23**(7) (2001) 850–856.
34. J. M. Soria, I. M. Díaz and J. H. García-Palacios, Vibration control of a time-varying modal-parameter footbridge: study of semi-active implementable strategies, *Smart Structures and Systems* **20**(5) (2017) 525–537.
35. F. Weber, Dynamic characteristics of controlled MR-STMDs of Wolgograd bridge, *Smart Materials and Structures* **22**(095008) (2013) p. 16pp.
36. F. Ferreira, C. Moutinho, Á. Cunha and E. Caetano, Use of Semi-Active Tuned Mass Dampers to Control Footbridges Subjected to Synchronous Lateral Excitation, *Journal of Sound and Vibration* (2018).
37. F. Ferreira and L. Simões, Optimum Design of a Controlled Cable Stayed Footbridge Subject to a Running Event using Semi-active and Passive Mass Dampers, *Journal*

of Performance of Constructed Facilities **33**(3) (2019) 1–14.
38. J. H. Koo, A. Shukla and M. Ahmadian, Dynamic performance analysis of non-linear tuned vibration absorbers, *Communications in Nonlinear Science and Numerical Simulation* **13**(9) (2008) 1929–1937.
39. J. Contreras-Lopez, F. Ornelas-Tellez and E. Espinosa-Juarez, Optimal control for footbridges' vibration reduction based on semiactive control through magnetorheological dampers, *International Journal of Structural Stability and Dynamics* **19**(09) (2019) p. 1950110.
40. F. Ferreira and L. Simões, Optimum design of a controlled cable-stayed footbridge subject to a running event using semiactive and passive mass dampers, *Journal of performance of constructed facilities* **33**(3) (2019) p. 04019025.
41. C. A. Barrera-Vargas, J. Naranjo-Pérez, I. M. Díaz and J. H. García-Palacios, Design of a Semiactive TMD for Lightweight Pedestrian Structures Considering Human-Structure-Actuator Interaction, *Actuators* **11** (mar 2022) p. 101.
42. J. M. Soria, I. M. Díaz and J. H. García-Palacios, Further steps towards the tuning of inertial controllers for broadband-frequency-varying structures, *Structural Control and Health Monitoring* **27**(1) (2020) p. e2461.
43. K. Van Nimmen, G. Lombaert, G. De Roeck and P. Van den Broeck, The impact of vertical human-structure interaction on the response of footbridges to pedestrian excitation, *Journal of Sound and Vibration* **402** (2017) 104–121.
44. A. Vijayan, N. Abraham and S. Kumari, Probabilistic sensitivity studies on modal properties and response of occupied pedestrian bridge (2021).
45. MATLAB, *version 7.10.0 (R2010a)* (The MathWorks Inc., Natick, Massachusetts, 2010).
46. R. W. Clough and J. Penzien, Dynamics of structures. Berkeley, *CA: Computers and Structures* (2003).
47. T. Asami and O. Nishihara, Closed-Form Exact Solution to H_∞ Optimization of Dynamic Vibration Absorbers (Application to Different Transfer Functions and Damping Systems), *Journal of Vibration and Acoustics* **125**(3) (2003) p. 398.
48. L. Chung, Y. Lai and C. Yang, Semi-active tuned mass dampers with phase control, *Journal of Sound and Vibration* **332**(15) (2013) 1–16.
49. C. Moutinho, Testing a simple control law to reduce broadband frequency harmonic vibrations using semi-active tuned mass dampers, *Smart Materials and Structures* **24**(5) (2015) 964–1726.
50. B. Peeters and G. De Roeck, Reference-based stochastic subspace identification for output-only modal analysis, *Mechanical systems and signal processing* **13**(6) (1999) 855–878.
51. Advanced load models for synchronous pedestrian excitation and optimised design guidelines for steel footbridges - SYNPEX, technical report, RWTH-Aachen University, Centre Technique Industriel de la Construction Métallique, TICM, Faculdade de Engenharia da Universidade do Porto and Schlaich Bergermann und Partner (2007).